




# A chemiresistive biosensor for detection of cancer biomarker in biological fluids using CVD-grown bilayer graphene

Mani Govindasamy<sup>1</sup> · Chen-Rong Jian<sup>1</sup> · Chang-Fu Kuo<sup>2</sup> · Ao-Ho Hsieh<sup>2</sup> · Jao-Liang Sie<sup>1</sup> · Chi-Hsien Huang<sup>1,2,3</sup> 

Received: 2 May 2022 / Accepted: 18 August 2022 / Published online: 7 September 2022  
© The Author(s), under exclusive licence to Springer-Verlag GmbH Austria, part of Springer Nature 2022

## Abstract

A chemiresistive biosensor is described for simple and selective detection of miRNA-21. We developed chemical vapor deposition (CVD) and low-damage plasma treatment (LDPT)-treated bilayer graphene composite of graphene oxide/graphene (GO/GR) for the determination of a reliable biomarker. We have successfully overcome the self-limiting growth mechanism by using CVD method to grow more than one layer of graphene on copper foil. In addition, LDPT can be used to form GO/GR structures for chemiresistive biosensor applications. Due to the direct formation of BLGR (bilayer graphene), the coupling between graphene layers is theoretically superior to that of stacked BLGR, which is also confirmed by the blue shift of the characteristic peak of graphene in Raman spectroscopy. The shift is about double compared with that of stacked BLGR. Based on the results, the limit of detection for the target miRNA-21 was calculated to be 5.20 fM and detection range is calculated as 100 fM to 10 nM, which is obviously better performance. Compared with previous work, this chemiresistive biosensor has good selectivity, and stability towards detection of miRNA-21. The ability to detect miRNA-21 in different biological fluids was almost identical to that in pH 7.4 phosphate-buffered saline (PBS). Thus, the proposed bilayer GO/GR of modified chemiresistive biosensor may potentially be applied to detect cancer cells in clinical examinations.

**Keywords** Bilayer graphene nanocomposite · Chemiresistive biosensors · Chemical vapor deposition · Detection of cancer cells · miRNA-21 determination

## Introduction

With an estimated 2.4 to 3 million incident cases, breast cancer is one of the major cancer in women. Approximately in the year of 2012 to 2019, 13 to 15% of women are diagnosed with breast cancer and 3% of women die with breast cancer [1]. The outbreak of the coronavirus disease (COVID-2019) caused by acute respiratory syndrome has endangered the health of people all over the world. Similarly, the mortality rate of cancer has been high in the world [2]. It is a disease caused by abnormal cell division, so the

human body has a chance to suffering from cancer disease and cure to become a major challenge in medical history [2]. When symptoms of cancer appear, it is usually in the middle and late stages, and the cancer cells at this stage have already begun to metastasize and spread to the whole body, which leads to difficulties in treatment. The most effective treatment method today is to perform excision treatment in the early stage of cancer. It is important to detect cancer cells in the body at an early stage. The most commonly, a breast cancer screening using mammography method or clinical breast examination [3]. However, this method must first find the tumor and takes a long time. miRNAs based biomarkers are an important class of small non-coding RNA involved in the regulation of gene expression. Their dysregulation has been related with Alzheimer's disease, rheumatic heart disease, malignancies, cardiovascular diseases, and different types of cancers [4]. Therefore, an in vitro biosensing of miRNAs that can be detected quickly has been developed based on various methods. In order to find the test substance for cancer cell detection, scientists found that certain malignant cells will selectively release specific "miRNA-21"

✉ Chi-Hsien Huang  
chhuang@mail.mcut.edu.tw

<sup>1</sup> Department of Materials Engineering, Ming Chi University of Technology, New Taipei City 243303, Taiwan

<sup>2</sup> Division of Rheumatology, Allergy and Immunology, Chang Gung Memorial Hospital, Taoyuan 33378, Taiwan

<sup>3</sup> Research Center for Intelligent Medical Devices, Ming Chi University of Technology, New Taipei City 243303, Taiwan

when studying of cancer cells [5]. The abnormal expression of miRNA-21 has a certain relationship and correlated with various cancer cells. Mainly, it also appears in a variety of cancers, such as lung cancer [6], esophageal cancer [7], and breast cancer [4]. Therefore, miRNA-21 is recognized as a typical cancer gene segment, and is often used as a biomarker for the detection of cancers.

MicroRNAs are fragments that circulate in the blood and present advantages such as low invasiveness and solution detection compared with traditional cancer analyses. However, most of methods have common limitations, such as low analytical throughput, low analytical efficiency, time, and labor consumption. In this work, hybridization chemiresistive biosensors have been developed, which are very attractive because of their high sensitivity and a simple sensing principle based on the change of resistance in response to the binding of target to active graphene materials.

To this end, this experiment developing on and improves on the previous research results of our laboratory and also other research articles [8]. Previously, graphene with good carrier mobility and high sensitivity due to its single element sublayer material properties was selected [9]. Because of the above characteristics, graphene/graphene oxide electrode materials are widely used in various fields such as supercapacitors [10], semiconductor applications [11], enzymatic [12], non-enzymatic electrochemical sensors [13], biosensors [14, 15], solar cells [16], and photocatalysis [17, 18]. According to the previous results, the application of stacked BLGR in chemiresistive biosensors and used to measure miRNA-21 achieved good results, but still compared with other biosensors with different structures of miRNAs, the analytical performance needs improvement. The coupling between graphene layers seems to be closely related to the sensitivity of subsequent components [8], so this experiment intends to use the CVD method to directly grow BLGR to increase the coupling between graphene layers. This can be achieved to improve the sensitivity and limit of detection (LOD) of miRNA-21 sensing.

Using CVD to prepare double-layer or even multi-layer graphene mostly adopts the growth method of cooling and precipitation, such as nickel [19]. Using this growth method will face many problems, such as catalysis, the thickness and purity of the metal directly affect the process conditions and precipitation conditions [20], and the rate and uniformity of cooling precipitation are not good [21, 22]. Another growth mechanism commonly used in the CVD process using catalytic metal copper (Cu) is much better. Due to its low carbon solubility, the growth method of growth and nucleation is adopted [23], and the reason why it is not often used to grow bilayer or multi-layer graphene is due to its unique self-limiting growth mechanism [24], but there have

been many researches in recent years. A method to break through this growth mechanism has been found by CVD method. By extending the time that the catalytic metal can catalyze [25], the graphene in the second layer has more time for nucleation and growth. Although there are still some mechanisms that need to be clarified, in a previously proposed growth method is referred [8] and developed further modification towards highly sensitive detection of miRNA-21. Benefiting from the strong chemiresistive biosensing amplification, the designed bilayer graphene sheets showed high sensitivity and selectivity for miRNA-21 detection. In this research work, we have developed a simple chemiresistive related biosensing platform for the detection of miRNA-21 in human albumin serum based on direct CVD-grown bilayer graphene sheets modified electrode.

## Experimental part

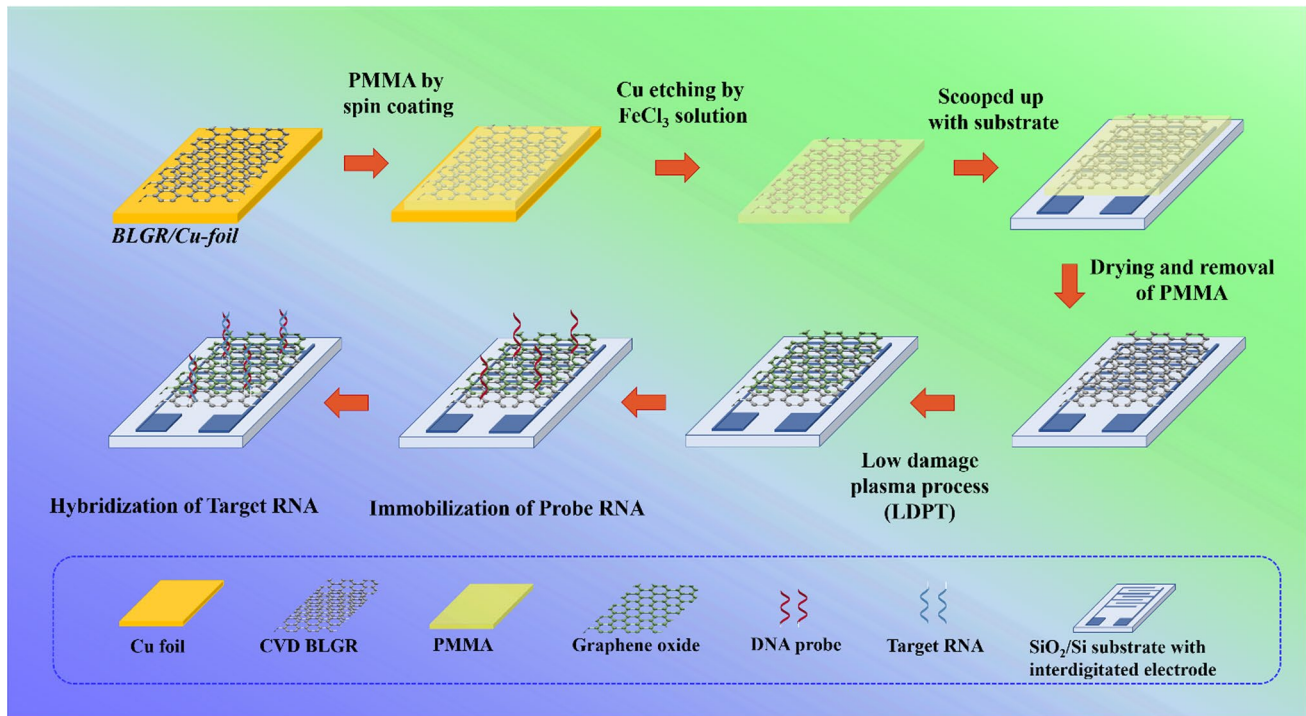
### Materials and reagents

miRNAs and DNA probes were purchased from Geomics Company (New Taipei City, Taiwan) and more details about RNAs were given in the supporting information (Table S1). Human serum albumin (HSA) and phosphate buffered saline (PBS, 0.1 mol L<sup>-1</sup>, pH 7.4) were purchased from Sigma-Aldrich. All other solvents and reagents were of analytical grade and used as received. A 25- $\mu$ m copper foil was purchased from Alfa Aesar (Thermo Fisher Scientific).

### Preparation of BLGR and GO/GR

Copper foil 15 cm  $\times$  20 cm is used into a quartz inner tube with a diameter of 6.5 cm, then put it into the CVD chamber, and use the pump to pump the chamber pressure to 5  $\times$  10<sup>-3</sup> torr. Pour 100 sccm of argon for 10 min to ensure that there is no impurity gas in the chamber to affect the subsequent process. Then, turn off the argon gas, raise the temperature to 945 °C and pass 200 sccm of hydrogen gas at the same time, and anneal for 35 min after reaching the target temperature to ensure that the internal temperature of the cavity is stable. The copper foil is oxidized due to exposure and the atmosphere is restored by hydrogen [8]. After entering the growth stage, methane was introduced, and the hydrogen was fixed at 40 sccm; the methane was adjusted according to the parameter requirements, and the pressure was maintained at 3.4 torr for 30 min. Finally, turn off all gases and remove the oven to quickly cool to room temperature.

Cr (5 nm) and Au (50 nm) thin films were deposited on the SiO<sub>2</sub>/Si substrate by thermal evaporation and through the mask of the interdigitated electrodes. Next, the BLGR



**Scheme 1.** Schematic diagram of CVD grown BLGR based on chemiresistive biosensors

is transferred from the copper foil to the electrode area on the gold interdigitated electrode by wet transfer, as shown in Scheme 1, and the annealing process is used to increase the adsorption between the BLG and the electrode and remove the polymer residues.

The GO/GR structure is prepared by grafting hydrogen–oxygen functional groups on graphene, and using the LDPT system to introduce hydrogen and oxygen gas mixture to prepare. The characteristics of treatment time [26] can effectively control the degree of graphene oxidation. The BLGR transferred to the gold-fingered electrode is oxidized, and only the upper graphene layer is modified, while the bottom graphene layer maintains the original structure to obtain the GO/GR structure.

### Immobilization and hybridization of probe DNA and miRNA

The PDMS prepared in advance was used to cut it into a rectangular box shape, which was fixed on a gold finger electrode with GO/GR structure, and 100  $\mu\text{L}$  of  $10^{-7}$  M probe modified with amino ( $-\text{NH}_2$ ) was added. DNA (purchased from Genomics) was dropped their into and left at room temperature for 16 h for immobilization. After the immobilization process, the electrode was rinsed three times with phosphate-buffered saline (PBS) to wash away the probe DNA with weak bonds and no bonds. Then, the electrode was placed in an environment of room temperature and miRNA-21 (purchased from Genomics)

of different concentrations was dropped for 4 h. During this stage, the sequence of the probe DNA would slowly unfold, and wait for the complementary sequences to interact with each other. Finally, rinsed 3 times with PBS aqueous solution to remove uncompleted hybridized miRNA-21. The measurement of the resistance change rate was performed using a Keithley 2000. After the electrode completes the probe immobilization process, the resistance value is measured first. The resistance value is the initial resistance of the element and is defined as  $R_0$ . Then, the component is subjected to a hybridization process, which will change the resistance value, and the resistance value after the change is defined as  $R$  [8]. Substitute the obtained two resistance values into the following formula (Eq. 1) to calculate the resistance change rate.

$$\left[ \frac{R - R_0}{R_0} \right] \times 100\% \quad (1)$$

The calculated result can be defined as the component's sensor response [27, 28].

## Results and discussion

### Investigate the effect of methane ratio on the number of graphene layers

In order to grow BLGR, it is very important that the nucleation sites of both layers are formed at the same time.

Therefore, this experiment mainly changed the proportion of methane in the process, which were 10%, 20%, and 40% respectively. To make more active carbon atoms diffuse between the first layer of graphene and the catalytic metal to increase the double, the probability that a layer nucleation point will occur. From Fig. 1A, Raman spectrum, it can be found that the ratio of  $I_{2D}/I_G$  gradually decreases from 0.96 to 0.73 with the increase of methane ratio [26], which means that the intensity of G peak increases; 2D peak intensity decreased. Both of these data are indicate an increase in the number of layers in graphene. The 2D peaks in the Fig. 1A can be found that there is a blue-shift phenomenon, and the occurrence of red-shift or blue-shift in the 2D peaks indicates that the carbon atoms are under the influence of stress [29]. Therefore, these results have a blue-shift phenomenon, which means that the coupling between graphene layers tends to increase. With the aid of the UV–Vis spectrum in Fig. 1, it can be found that the transmittance gradually decreased from 95.5 to 93.1%. This result is consistent with the results of Raman spectroscopy (Fig. 1A), which both show that the thickness of graphene increases with the increase of methane ratio, which also proves that it is feasible to increase the thickness of graphene by increasing the ratio of methane.

From Fig. 1C, in the optical microscope (OM) image of graphene layers, it can be found that after observing its surface morphology, it is not difficult to find the phenomenon of different darkness's, so the Raman spectrum analysis is carried out for regions with different depths (Fig. 1F). The  $I_{2D}/I_G$  ratio of the light part is about 1.34 (black circle part), the dark part is about 0.98 (red circle part), and the boundary between dark and light is less obvious. It can be observed in the OM image of Fig. 1D, that the light-colored area tends to shrink and form small spots, the boundary between the dark and the light becomes more obvious, and a darker area appears with an  $I_{2D}/I_G$  ratio of about 0.79 (blue circles part). Finally, in the OM map in Fig. 1E, it can be observed that the light-colored spots almost disappeared, and the dark-colored areas increased significantly (blue circles) almost covering the entire OM map. This phenomenon means that the coverage of BLGR grown by this method can be adjusted. Although, the penetration rate of this set of parameters with a methane ratio of 10% is the closest to that of BLGR in the literature, its single-layer graphene coverage rate is high, which will be a major obstacle to the subsequent plasma process. Therefore, the subsequent experiments are carried out with the parameters of methane ratio of 20%. On the one hand, it can reduce the influence of plasma damage, and on the other hand, it can increase the operating space during the process, as shown in Raman mapping (Figure S1). Based on this data, BLGR coverage is calculated to be about 80% [27]. The group of parameters of 40% methane is not used,

because although the influence of plasma damage is theoretically the least among the three groups of parameters, graphene with a higher average thickness will increase the difficulty of plasma modification and also reduces the sensitivity of the sensing element. The size of the copper foil used in the CVD process this time is  $20 \times 15 \text{ cm}^2$ , so the BLGR on the copper foil is divided into three parts: the intake end, the middle end and the exhaust end for UV–Vis measurement. Figure S2 shows and ensure that the penetration rates of the three zones are consistent. The optical transmittances are 94.5%, 94.4%, and 94.3%, respectively, and the difference between the front and rear ends is not more than 0.2%, which proves that this method can be used in such a large-area process and also maintain a certain stability.

TEM and AFM images were also used to analyze the BLGR prepared in this way. The TEM image of BLGR (Fig. 2A–C) is analyzed based on the distance between its layers. The theoretical value in the literature is about 0.34 nm [30], while the result in this experiment is about 0.35 nm, which is very close to the values in the literature. From Fig. 2D–F, in the AFM image of BLGR, the film thickness is analyzed by the height difference between BLGR and substrate  $\text{SiO}_2$ . From the figure, it can be found that the edge of the BLGR film and the junction of the substrate will easily have a sudden height increase. This happens because the edges are prone to breakage, warping, and curling when the BLGR is cut and picked up from the deionized water during the wet transfer process, which in turn makes it difficult for chemicals to be absorbed. When calculating the height difference this time, the left and right measurements of the BLGR edge are used as the reference value for calculation, and the result of this experiment is about 0.8 nm. The thickness of graphene in the literature is about 0.37 nm; BLGR is about 0.8 nm [31]. The experimental results are very close to the theoretical value, which also confirms the successful preparation of BLGR by chemical vapor deposition.

### Comparison of BLGR properties with different preparation methods

According to the results in the “[Investigate the effect of methane ratio on the number of graphene layers](#)” section, it is proved that the strategy of increasing the proportion of carbon source in the process to obtain double-layer and multi-layer graphene is feasible, so the next step is discussed, as shown in Fig. 3A and A'. Raman spectra of BLGR obtained for single-layer graphene and different preparation methods. According to the literature, the  $I_{2D}/I_G$  ratio of the Raman spectrum of BLGR is around 1 [25], and the red line in the figure below (Fig. 3A) is the BLGR formed by the single-layer graphene after two wet transfer stacking and annealing process. It can be found

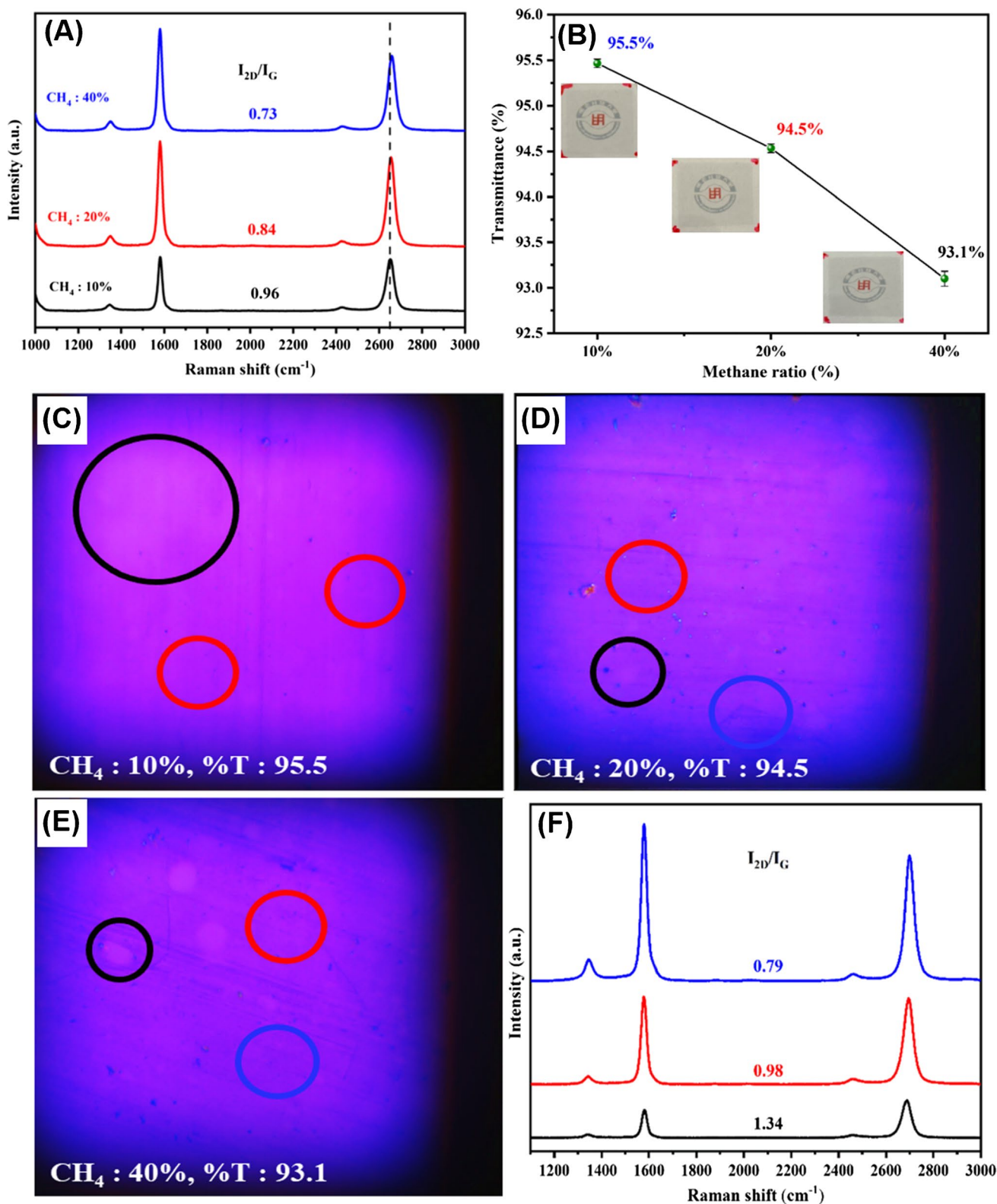


**Fig. 1** A Raman spectrum of BLGR prepared under different process conditions and B Calibration plot between UV-Vis transmittance and different methane ratios. C OM images of 10%, D 20%, and E 40% methane and F Raman spectra of different methane ratios

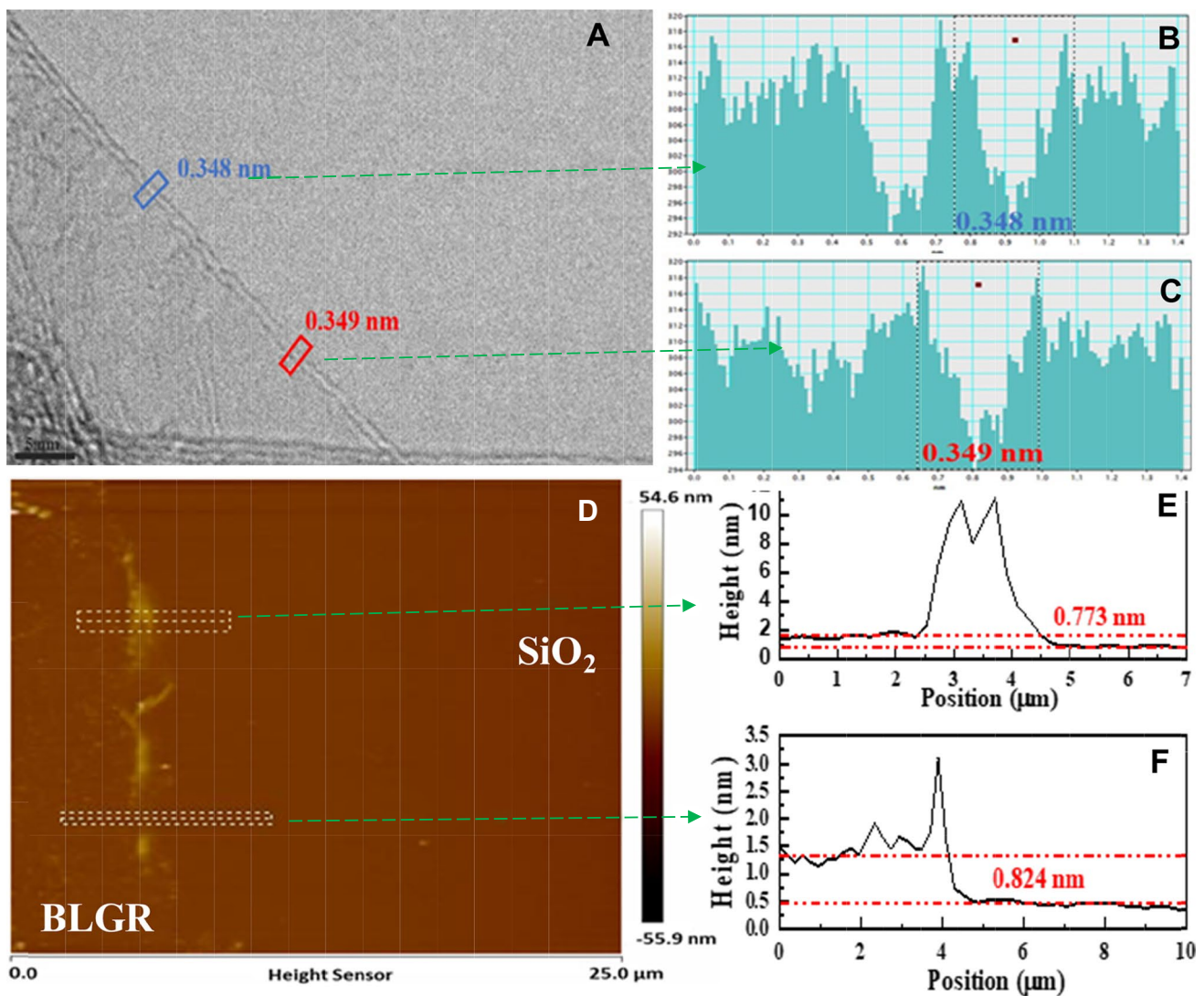


**Fig. 2** TEM (A–C) and AFM (D–F) analysis of BLGR

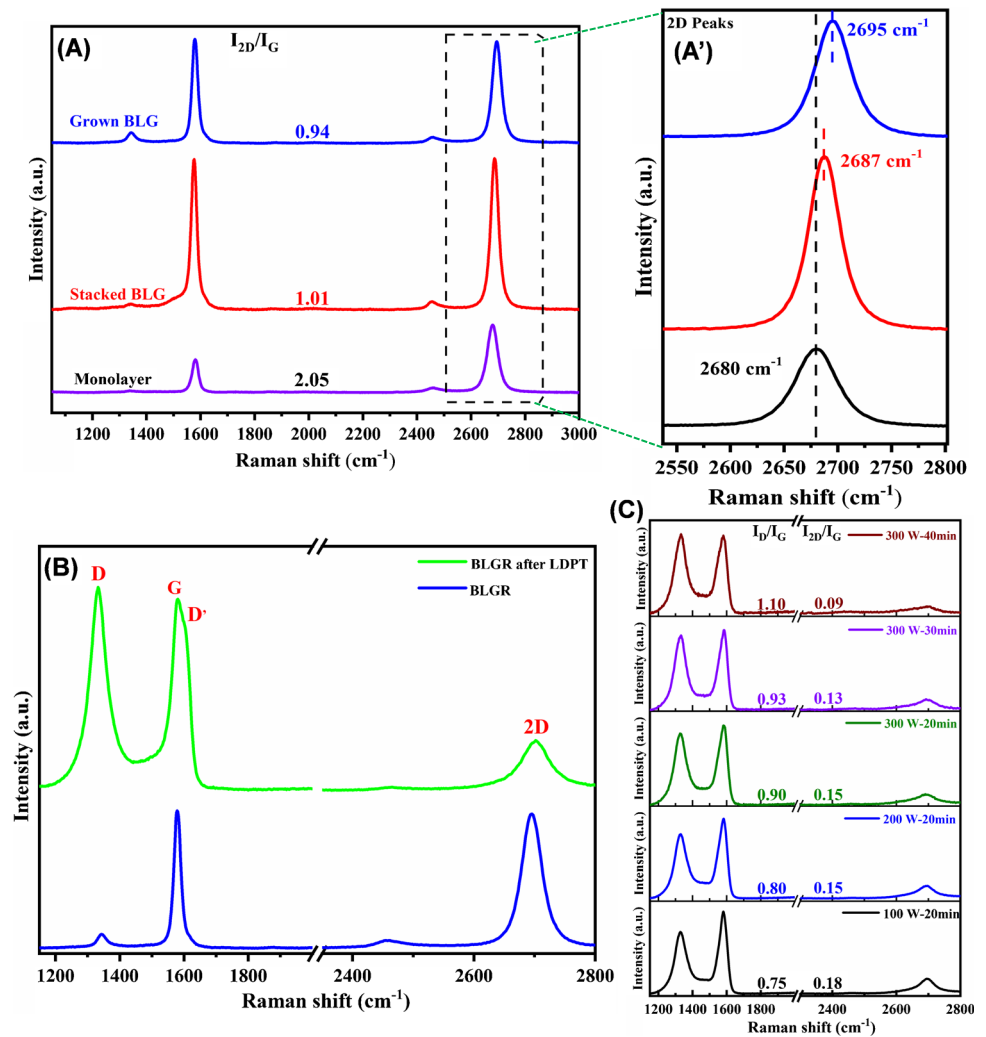
that  $I_{2D}/I_G$  ratio of 1.01 is slightly higher than the literature value. The Raman diagram of the blue line is the BLGR processed by adjusting the ratio of hydrogen and methane. Its  $I_{2D}/I_G$  ratio of 0.94 is closer to the literature than the stacked one. Therefore, good formation is based on direct growth of graphene layers. Because, the directly grown BLGR layers are between the layers by CVD method. The coupling of the graphene is better than that of the stacking process, which can also be proved by the obvious blue shift of the 2D peak. The BLGR blue shift of the single-layer graphene and the stacking process is around  $8\text{ cm}^{-1}$ ; the blue shift of the directly grown BLGR is around  $16\text{ cm}^{-1}$ , and the difference between the two is about double. The position of the 2D peak of the directly grown BLGR is also close to the literature, and the literature value is around  $2698\text{ cm}^{-1}$  [32]. From this, a conclusion can be drawn

that the coupling property of the directly prepared BLGR is better than that of the stacked BLGR, and it is shown from the previous research [8] that the improvement of the coupling property of graphene. It is useful for the subsequent application as a biosensing element. It may be certain influence towards detection of miRNA based on chemiresistive biosensors.

### Preparation of GO/GR structure and optimization

The GO/GR structure is obtained by wet transfer of BLGR onto a  $\text{SiO}_2$  substrate with gold interdigitated electrodes and then through annealing process and LDPT surface modification is shown in Fig. 3B. The plasma modification conditions of the stacking process BLGR were previously treated. After plasma modification, it can be observed that there is

**Fig. 3** **A** and **A'** Raman spectra of graphene obtained different preparation methods. **B** Raman analysis of BLGR and surface modified BLGR. **C** Raman spectra based on optimization of radio-frequency power and plasma modification time

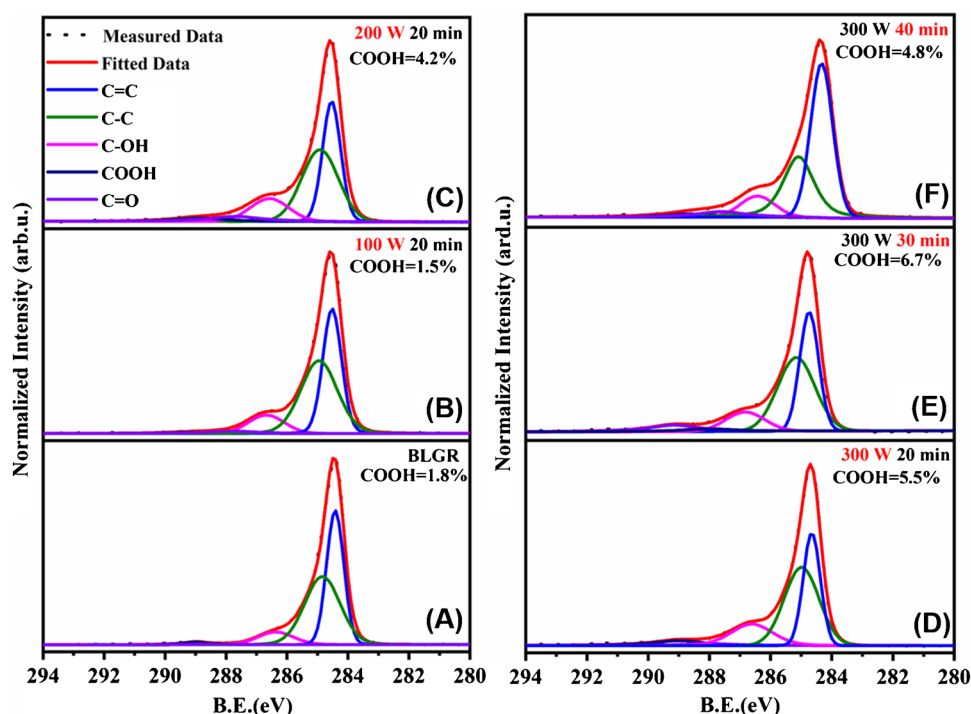


an obvious D' peak next to the G peak that is not completely combined with the G peak, and the 2D peak can still be clearly observed. The existence of these two information indicates that there is still room for adjustment and optimization of the plasma conditions. In order to optimize the plasma parameters, so that the BLGR can achieve the best oxidation effect, the plasma parameters of the BLGR formed by the previous stacking process are used as the basis and optimized. Five groups of different parameters were used to adjust their radio-frequency power (RF) or plasma modification time and the obtained materials were analyzed by Raman and X-ray photoelectron spectroscopy (XPS). From the Raman spectra in Fig. 3C and 3D, it can be observed that with the increase of radio frequency power or plasma modification time. The gradually decreasing a peak intensity and the gradually increasing  $I_D/I_G$  both represent the increase of structural defects that may mainly resulting from the incorporation of the oxidative functional groups in the carbon lattices, which will be discussed in Fig. 4. At the same time, it can be found that the increase in D, the same result is also

reflected by the gradually increasing full width at half maximum of the peak fully integrated with the G peak, and the 2D peak also gradually disappears with increasing degree of surface modification.

Different bonds have different binding energies, so XPS spectroscopy was used to analyze the content of different bonds on the GO structure, since the carboxyl group (-COOH) in the GO structure can undergo a dehydration reaction with the biomolecules of the modified amino group (-NH<sub>2</sub>) and generate a bond [33]. Theoretically, the carboxyl group content on the GO structure can be related to the probe of the modified amino group. The content of needle DNA is proportional, so the content of carboxyl groups on the GO structure will greatly affect the measurement results of subsequent sensing elements. Figure 4A–F image shows the overlay of XPS spectra with different plasma parameters. It can be found that with the increase of RF power or plasma modification time, the proportion of carboxyl groups also increases, up to 6.7%. It is worth noting that the parameters of RF power

**Fig. 4** A–F Are the overlay of XPS spectra at C1s with different plasma parameters



300 W, plasma modification time 40 min, and the content of carboxyl groups dropped significantly. It is speculated, because the degree of plasma modification of BLGR is too high, which makes the structure of BLGR suffer. When severe damage affects the content of carboxyl groups, the content of carboxyl groups does not increase but decreases, which can also be reflected from the Raman spectrum and XPS full spectrum in Figs. 4D and S3. It can be observed that the 2D peak of the GO/GR structure under this parameter almost disappears. The intensity of the Raman signal is much weaker than other parameters, and it can be observed in the XPS full spectrum that with the increase of the degree of plasma modification and the substrate SiO<sub>2</sub>. The proportion is getting higher and the overall carbon content is getting lower, and only 40% is left. In order to prove that the amino group on the probe DNA and the carboxyl group on the GO structure undergo a dehydration reaction to form a bond, Figure S4 is a full spectrum scan using XPS after the immobilization process. It can be observed that after the immobilization process, although it is not obvious but a peak representing N1s appears. In Figure S5, obvious NH-CO bonds can also be observed after the immobilization process [34]. From these results, it is shown that the probe DNA is linked to GO through amino groups and structure can create bonds. In addition, this experiment also used the Coulomb chronometric method in electrochemistry to calculate the probe density of each parameter, and the results were basically consistent with XPS and Raman spectroscopy.

#### Detection of different concentrations of miRNA-21 based on resistance change rate

In order to verify, the GO/GR structure can be applied in chemiresistive biosensing elements (miRNA-21), and concentrations of 10 nM, 1 nM, 100 pM, 10 pM, 1 pM, and 100 fM were hybridized in this experiment. The concentration of the analyte is diluted with 1xPBS aqueous solution. In order to determine whether the 1xPBS aqueous solution will affect the measurement results (see Figure S6), the 1xPBS aqueous solution is used as the analyte to measure the resistance change rate. From the results, it can be observed the average resistance change rate of 1xPBS is about 1.1%. Although there is still a slight resistance change, the overall impact is not large, and the measurement results on different test pieces are very close, which means that this biosensing element, and the measurement results have a certain uniformity. Figure 5A shows the resistance change rate of miRNA-21 at different concentrations and the results are increases linearly with the logarithm of the concentrations. Because, the negatively charged miRNA-21 is hybridized with the DNA probe attached to the GO/GR results in the decrease of hole carrier concentration and mobility of the sensing element. As the concentration of the analyte increases, more miRNA-21 will hybridize with the probe DNA, and the resistance increases. When the highest concentration of 10 nM is detected, the resistance change rate can be as high as 13.6%, which means that it can be easily detected by sensing element at this concentration.



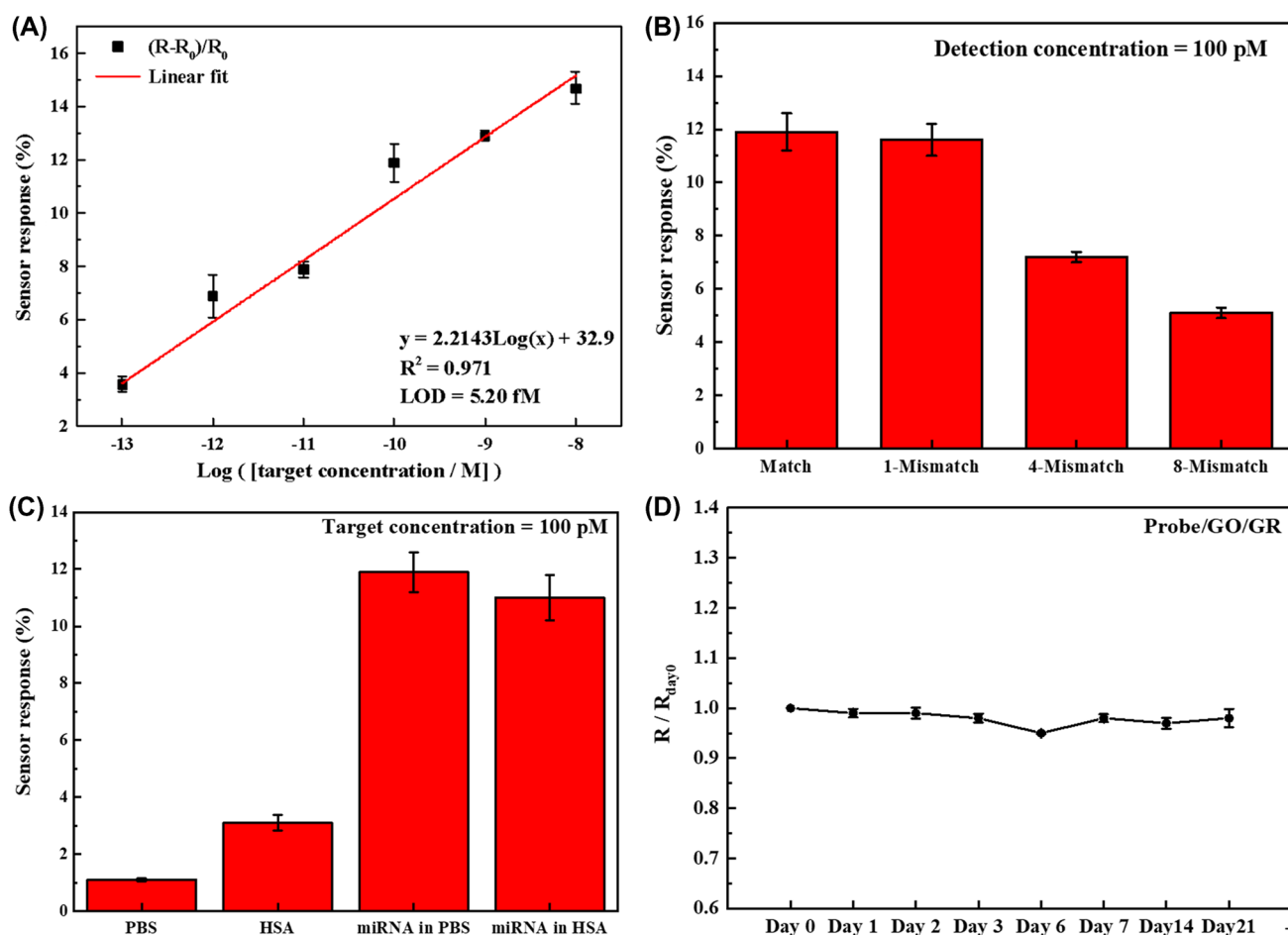


**Fig. 5** **A** Trend diagram of resistance change rate with different concentrations of miRNA-21 hybridization. **B** Selectivity analysis of miRNA-21 sensing elements. **C** Real sample analysis in HAS and **D** stability analysis of probe/GO/GR

The resistance change rate obtained by detecting different concentrations of miRNA-21 can be calculated by Eq. 1, and the lowest concentration (limit of detection; LOD) that can be detected by this sensing element can be calculated using Eq. 2.

$$Y = B + 3 \times SD \tag{2}$$

$B$  = the effect of 1xPBS on the element during the hybridization process,  $SD$  = standard deviation. Substitute the detected resistance change rate of 1xPBS into the above formula, then can obtain  $Y = 1.271$ , and substitute the  $Y$  value back into the linear equation obtained by detecting 6 different concentrations in Fig. 5A and the calculated the  $x$  value is the lowest measurable concentration value, which is calculated by following Eq. 3.

$$1.271068 = 2.2143 \log(x) + 32.9 \tag{3}$$

The limit of detection is calculated as 5.20 fM and this result is compared with the previous studies done in our

laboratory [8]. The results of this study can be found to have higher rates of change at each concentration than previous studies, and also the sensitivity of the sensor and limit of detection is extremely good performance compared with previous articles [27, 28].

### Selectivity and real sample analysis of miRNA-21 sensing

In addition to the detection limit, selective measurement is also a very important indicator to determine whether the biosensor is good or bad. If the selectivity of the biosensor is not good, it will be impossible to clearly determine whether the measurement result is affected by the object to be tested or not. Caused by other substances, resulting in a lack of confidence in the final measurement results. In order to determine the selectivity of the sensor, GO/GR structure is applied to chemiresistive biosensing elements, and three miRNAs with different partial sequence arrangement from the analyte miRNA-21 were used in this

experiment, namely 1-mismatch, 4-mismatch, and 8-mismatch which are measured at a concentration of 100 pM. The sequence mismatch will increase the difficulty of successful hybridization of the analyte and the probe DNA during the hybridization stage, or the analyte cannot be completely matched and cannot be hybridized. It can be found from Fig. 5B, the rate of change of resistance has a decreasing trend as the partially mismatched sequence increases and this result is expected for the reasons stated above. Compared with miRNA-21, the observed resistance change rate in 1-mismatch is similar to that of miRNA-21. It is presumed that only one sequence does not match. It is difficult to imagine that this sequence will directly affect the other 21 sequences that match each other. Therefore, the difficulty of matching increases and the phenomenon of inability to heterozygosity is unlikely to occur here in theory. Another evidence to support this argument is that in the resistance change rate of 8-mismatch, the 8 mismatched sequences are already close to half of all sequences, and their average resistance change rate is reduced to about half of the original, which means that the heterozygous difficulty is greatly increased. Due to the increase, it can be expected that the resistance change rate will drop to about 1 ~ 2% (the change rate comes from PBS) when the sequences are completely non-complementary. Based on this experiments, our modified electrode has good selectivity and detection ability towards miRNA-21.

The sensing analysis of the sensing element in this experiment was carried out on miRNA-21 in the return of PBS solution. However, the environment in the human body is much more complex than that in PBS. In order to verify whether this sensing element has the potential to be applied to the human body, the PBS aqueous solution is replaced with human serum albumin (HSA), which is more complex and closer to the human environment for interference aspect and detection. miRNA-21 was diluted to 100 pM with HSA and compared with the results in the PBS environment. It can be observed from Fig. 5C, that the resistance change rate in HSA is slightly lower. It is speculated performance in HSA conditions, because HSA has more interfering substances and impurities than PBS, so it will hinder miRNA-21 paired with the probe DNA, which in turn affected the subsequent resistance changes. As far as the results are concerned, the rate of change in HSA is only reduced by about one percent, which proves that although the sensing element will be disturbed due to different sensing environments, the overall impact is not large, and the under-test can still be clearly detected. rate of change of resistance. It is worth noting that when using HSA, due to its high impurities, it is easy to physically adsorb on the electrode surface. Therefore, the cleaning action before measuring the resistance value needs to be repeated several times to avoid affecting the subsequent measurement.

## Stability analysis of BLGR modified biosensor towards miRNA-21 detection

Practically speaking, biosensors are unlikely to be used directly after being prepared. Most of the time between preparation and use will pass through transportation or waiting, so the time that biosensors can be stored for is quite important. In this experiment, after the electrode was immobilized (probe/GO/GR/electrode), 1xPBS aqueous solution was dropped and placed at room temperature for storage, and its resistance change was measured every day. The purpose of dropping pure PBS aqueous solution was to avoid biomolecules on the element come into contact with air. It can be observed from Fig. 5D that even after 3 weeks (21 days) of placement, the resistance change is still very stable and does not fluctuate too much. In order to further test whether the probe DNA is still active, place one, four, and one. The 7-day biosensing element is hybridized. From Figure S7, it can be found that the resistance change rate of the hybridization process after being placed for 7 days of miRNA-21/probe/GO/GR and the resistance change rate of the hybridization process directly after the component preparation is only about one modified electrode. This result proves that the biosensor can maintain good stability and activity even after 7 days.

## Conclusion

In this study, bilayer graphene of GO/GR was successfully prepared by adjusting the ratio of methane in the control process. The number of layers and surface morphology were analyzed by Raman spectroscopy, optical microscopy, UV-Vis spectroscopy, AFM, and TEM. The blue-shift phenomenon of the 2D peak of BLGR in the Raman spectrum shows that the directly grown BLGR has better interlayer coupling. The GO/GR structure was prepared by the LDPT system, and a series of nanomaterial analyses such as Raman spectroscopy, XPS, and chrono Coulomb method were used to optimize the plasma process conditions. Finally, the prepared GO/GR structure was applied to the biosensing element to detect miRNA-21 for measuring of detection limit, selectivity, and stability. To compare with the GO/GR structure using the stacking process, from the results of detecting miRNA-21 in different concentration ranges, it is known that its sensitivity and detection limit are better than those of the stacking process due to the improved coupling between layers, and the developed sensor detection limit is 5.2 fM with linear measurement range is 100 fM to 10 nM, although it can be seen from the results that the sensing of element in this experiment has better biosensor performance compared than the previous research articles. It cannot be ignored that the BLGR coverage, still need to be improvement, so how to prepare a high-coverage sensors based on BLGR will be the next research topic of my research group.

**Supplementary Information** The online version contains supplementary material available at <https://doi.org/10.1007/s00604-022-05463-7>.

**Funding** This study was funded by the Ministry of Science and Technology under grant number 107–2221-E-131–011 and National Science and Technology Council of Taiwan under grant number 111–2811-E-131–003.

## Declarations

**Conflict of interest** The authors declare no competing interests.

## References

- Pimalai D, Putnin T, Waiwinya W, Chotsuwan C, Aroonyadet N, Japrun D (2021) Development of electrochemical biosensors for simultaneous multiplex detection of microRNA for breast cancer screening. *Microchim Acta* 188:1–10
- Bray F, Ferlay J, Soerjomataram I, Siegel RL, Torre LA, Jemal A (2018) Global cancer statistics 2018: GLOBOCAN estimates of incidence and mortality worldwide for 36 cancers in 185 countries. *CA: a Cancer J Clin* 68:394–424
- Warner E, Plewes D, Shumak R, Catzavelos G, Di Prospero L, Yaffe M, Goel V, Ramsay E, Chart P, Cole D (2001) Comparison of breast magnetic resonance imaging, mammography, and ultrasound for surveillance of women at high risk for hereditary breast cancer. *J Clin Oncol* 19:3524–3531
- Gutiérrez-Gálvez L, García-Mendiola T, Gutiérrez-Sánchez C, Guerrero-Esteban T, García-Diego C, Buendía I, García-Bermejo ML, Pariente F, Lorenzo E (2021) Carbon nanodot-based electrogenerated chemiluminescence biosensor for miRNA-21 detection. *Microchim Acta* 188:1–12
- Xiao Q, Li J, Jin X, Liu Y, Huang S (2019) Ultrasensitive electrochemical microRNA-21 biosensor coupling with carboxylate-reduced graphene oxide-based signal-enhancing and duplex-specific nuclease-assisted target recycling. *Sens Actuators B: Chem* 297:126740
- Alberg AJ, Samet JM (2003) Epidemiology of lung cancer. *Chest* 123:21S–49S
- Enzinger PC, Mayer RJ (2003) Esophageal cancer. *N Engl J Med* 349:2241–2252
- Huang C-H, Huang T-T, Chiang C-H, Huang W-T, Lin Y-T (2020) A chemiresistive biosensor based on a layered graphene oxide/graphene composite for the sensitive and selective detection of circulating miRNA-21. *Biosens Bioelectron* 164:112320
- Li X, Zhu Y, Cai W, Borysiak M, Han B, Chen D, Piner RD, Colombo L, Ruoff RS (2009) Transfer of large-area graphene films for high-performance transparent conductive electrodes. *Nano Lett* 9:4359–4363
- Athanasiou M, Samartzis N, Sygellou L, Dracopoulos V, Ioannides T, Yannopoulos SN (2021) High-quality laser-assisted biomass-based turbostratic graphene for high-performance supercapacitors. *Carbon* 172:750–761
- Shanmugam M, Jacobs-Gedrim R, Song ES, Yu B (2014) Two-dimensional layered semiconductor/graphene heterostructures for solar photovoltaic applications. *Nanoscale* 6:12682–12689
- Mani V, Govindasamy M, Chen S-M, Chen T-W, Kumar AS, Huang S-T (2017) Core-shell heterostructured multiwalled carbon nanotubes@ reduced graphene oxide nanoribbons/chitosan, a robust nanobiocomposite for enzymatic biosensing of hydrogen peroxide and nitrite. *Sci Rep* 7:1–10
- Govindasamy M, Rajaji U, Wang S-F, Chang Y-J, Ramalingam RJ, Chan C-Y (2020) Investigation of sonochemically synthesized sphere-like metal tungstate nanocrystals decorated activated carbon sheets network and its application towards highly sensitive detection of arsenic drug in biological samples. *J Taiwan Inst Chem Eng* 114:211–219
- Mani V, Devasenathipathy R, Chen S-M, Subramani B, Govindasamy M (2015) A novel glucose biosensor at glucose oxidase immobilized graphene and bismuth nanocomposite film modified electrode. *Int J Electrochem Sci* 10:691–700
- Lahcen AA, Rauf S, Aljedaibi A, de Oliveira Filho JI, Beduk T, Mani V, Alshareef HN, Salama KN (2021) Laser-scribed graphene sensor based on gold nanostructures and molecularly imprinted polymers: application for Her-2 cancer biomarker detection. *Sensors Actuators B: Chem* 347:130556
- Fernández-Arteaga Y, Maldonado J-L, Nicasio-Collazo J, Meneses-Nava M-A, Rodríguez M, Barbosa-García O, Sierra U, Fernández S, Frontana-Urbe BA (2021) Solution processable graphene derivative used in a bilayer anode with conductive PEDOT: PSS on the non-fullerene PBDB-T: ITIC based organic solar cells. *Sol Energy* 225:656–665
- Taniguchi T, Nurdwijayanto L, Li S, Lim HE, Miyata Y, Lu X, Ma R, Tang D-M, Ueda S, Tsukagoshi K (2020) On/Off boundary of photocatalytic activity between single-and bilayer MoS<sub>2</sub>. *ACS Nano* 14:6663–6672
- Kumar KY, Parashuram L, Prashanth M, Kumar CP, Alharti FA, Krishnaiah P, Jeon B-H, Govindasamy M, Raghu M (2021) N-doped reduced graphene oxide anchored with δTa<sub>2</sub>O<sub>5</sub> for energy and environmental remediation: efficient light-driven hydrogen evolution and simultaneous degradation of textile dyes. *Adv Powder Technol* 32:2202–2212
- Wang X, Zhi L, Müllen K (2008) Transparent, conductive graphene electrodes for dye-sensitized solar cells. *Nano Lett* 8:323–327
- Giamini SA, Marquez-Velasco J, Sakellis I, Tshipas P, Kelaidis N, Tsoutsou D, Boukos N, Kantarelou V, Xenogiannopoulou E, Speliotis T (2016) Experimental investigation of metallic thin film modification of nickel substrates for chemical vapor deposition growth of single layer graphene at low temperature. *Appl Surf Sci* 385:554–561
- Reina A, Thiele S, Jia X, Bhaviripudi S, Dresselhaus MS, Schaefer JA, Kong J (2009) Growth of large-area single-and bi-layer graphene by controlled carbon precipitation on polycrystalline Ni surfaces. *Nano Res* 2:509–516
- Zhang Y, Gomez L, Ishikawa FN, Madaria A, Ryu K, Wang C, Badmaev A, Zhou C (2010) Comparison of graphene growth on single-crystalline and polycrystalline Ni by chemical vapor deposition. *The Journal of Physical Chemistry Letters* 1:3101–3107
- Gao Y, Liu Z, Sun D-M, Huang L, Ma L-P, Yin L-C, Ma T, Zhang Z, Ma X-L, Peng L-M (2015) Large-area synthesis of high-quality and uniform monolayer WS<sub>2</sub> on reusable Au foils. *Nat Commun* 6:1–10
- Negishi R, Hirano H, Ohno Y, Maehashi K, Matsumoto K, Kobayashi Y (2011) Layer-by-layer growth of graphene layers on graphene substrates by chemical vapor deposition. *Thin Solid Films* 519:6447–6452
- Liu L, Zhou H, Cheng R, Yu WJ, Liu Y, Chen Y, Shaw J, Zhong X, Huang Y, Duan X (2012) High-yield chemical vapor deposition growth of high-quality large-area AB-stacked bilayer graphene. *ACS Nano* 6:8241–8249
- Huang C-H, Su C-Y, Lai C-S, Li Y-C, Samukawa S (2014) Ultra-low-damage radical treatment for the highly controllable oxidation of large-scale graphene sheets. *Carbon* 73:244–251
- Shen Y, Tran T-T, Modha S, Tsutsui H, Mulchandani A (2019) A paper-based chemiresistive biosensor employing single-walled carbon nanotubes for low-cost, point-of-care detection. *Biosens Bioelectron* 130:367–373

28. Shen Y, Tran T-T, Modha S, Tsutsui H, Mulchandani A (2018) A paper-based chemiresistive biosensor employing single-walled carbon nanotubes for low-cost, point-of-care detection. *Biosens Bioelectron* 130:367–373
29. Ni Z, Wang Y, Yu T, You Y, Shen Z (2008) Reduction of Fermi velocity in folded graphene observed by resonance Raman spectroscopy. *Phys Rev B* 77:235403
30. Popov AM, Lebedeva IV, Knizhnik AA, Lozovik YE, Potapkin BV, Poklonski NA, Siahlo AI, Vyrko SA (2013) AA stacking, tribological and electronic properties of double-layer graphene with krypton spacer. *J Chem Phys* 139:154705
31. Shen Z, Li J, Yi M, Zhang X, Ma S (2011) Preparation of graphene by jet cavitation. *Nanotechnology* 22:365306
32. Zeng J, Liu J, Zhang S-X, Zhai P-F, Yao H-J, Duan J-L, Guo H, Hou M-D, Sun Y-M (2015) Irradiation effects of graphene and thin layer graphite induced by swift heavy ions. *Chin Phys B* 24:086103
33. Rodríguez S, Makinistian L, Albanesi E (2016) Theoretical study of the adsorption of histidine amino acid on graphene. *Journal of Physics: Conference Series*, IOP Publishing, pp. 012012
34. Zhuang W, He L, Zhu J, Zheng J, Liu X, Dong Y, Wu J, Zhou J, Chen Y, Ying H (2016) Efficient nanobiocatalytic systems of nuclease P1 immobilized on PEG-NH<sub>2</sub> modified graphene oxide: effects of interface property heterogeneity. *Colloids Surf, B* 145:785–794

**Publisher's note** Springer Nature remains neutral with regard to jurisdictional claims in published maps and institutional affiliations.

Springer Nature or its licensor holds exclusive rights to this article under a publishing agreement with the author(s) or other rightsholder(s); author self-archiving of the accepted manuscript version of this article is solely governed by the terms of such publishing agreement and applicable law.